iScience

CellPress
OPEN ACCESS

Article

The role of chirality and plastic crystallinity in the optical and mechanical properties of chlorosomes

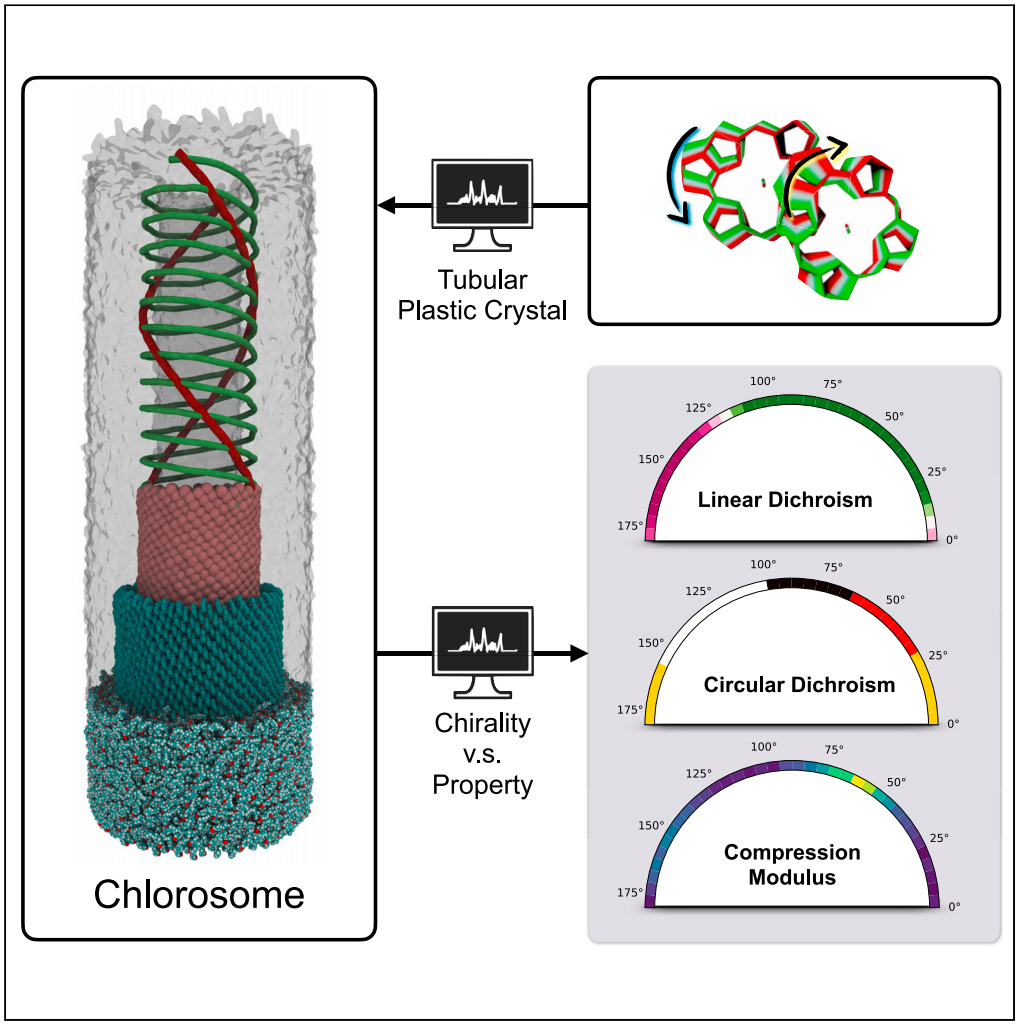

Xinmeng Li, Francesco Buda, Huub J.M. de Groot, G. J. Agur Sevink

xinmeng.li@kjemi.uio.no (X.L.)
a.sevink@chem.leidenuniv.nl (G.J.A.S.)

Highlights

Classifies chlorosomes in terms of a tubular plastic crystal phase

Clarifies the unique strategy of chlorosomes for harvesting and transporting energy

Presents a protocol for building atom-resolved helical tube structures

Maps tube chirality directly to measurable optical and mechanical responses

Li et al., iScience 25, 103618
January 21, 2022 © 2021 The Authors.
https://doi.org/10.1016/j.isci.2021.103618

iScience

CellPress
OPEN ACCESS

Article

The role of chirality and plastic crystallinity in the optical and mechanical properties of chlorosomes

Xinmeng Li,[1,2,*] Francesco Buda,[1] Huub J.M. de Groot,[1] and G. J. Agur Sevink[1,3,*]

SUMMARY

The most efficient light-harvesting antennae found in nature, chlorosomes, are molecular tubular aggregates (TMAs) assembled by pigments without protein scaffolds. Here, we discuss a classification of chlorosomes as a unique tubular plastic crystal and we attribute the robust energy transfer in chlorosomes to this unique nature. To systematically study the role of supramolecular tube chirality by molecular simulation, a role that has remained unresolved, we share a protocol for generating realistic tubes at atomic resolution. We find that both the optical and the mechanical behavior are strongly dependent on chirality. The optical-chirality relation enables a direct interpretation of experimental spectra in terms of overall tube chirality. The mechanical response shows that the overall chirality regulates the hardness of the tube and provides a new characteristic for relating chlorosomes to distinct chirality. Our protocol also applies to other TMA systems and will inspire other systematic studies beyond lattice models.

INTRODUCTION

Molecular assemblies that are held together by non-covalent interactions between flexible molecular building blocks offer the potential to modulate emergent mechanical, electrical, optical, or other functional properties via molecular rearrangements (Das et al., 2020; Mattia and Otto, 2015; Saikin et al., 2013). A responsive nature of building blocks, both in terms of tuning and switching of ensemble properties by environmental conditions and of molecular properties by the ensemble, is particularly advantageous in biology, where the fluxes and conditions at the interface between functional domains like organelles change across spatial and temporal scales (Badeau and DeForest, 2019; Egan et al., 2015). A characteristic example of a multiple-scale response of such a "responsive matrix" can be observed in photosynthetic processes (Purchase et al., 2019). Here, on the one hand, thermally induced molecular vibrations in nanostructured arrays of protein matrices mediate efficient transfer of excitation energy between cofactors by resonant coupling to pairs of electronic degrees of freedom at thermally induced level crossings (Romero et al., 2014; Scholes et al., 2017), and on the other hand, on a much larger length and timescale, the fluidic membrane scaffold that hosts these complexes in chloroplasts responds to an excessive incoming photon flux by a dissipative structural rearrangement or remodeling of the structure (Stingaciu et al., 2016). While the sensitivity to variation poses a challenge for any type of structural rearrangement to take place, the real caveat is in the magnitude of the thermodynamic forces that drive the remodeling process, because they are usually quite small. The result is a very sluggish remodeling process at larger length scales in crowded or dense molecular systems when additional driving forces are absent, especially in the vicinity of a critical point where critical slowing down takes place. To function as an effective switch, the time, length, and energy scales involved in switching should be matched.

It is increasingly realized that biology, where vital processes require highly coordinated structural transitions at low energetic costs, often exploits a proximity to phase boundaries to solve the issue of sensitivity, because this permit large "effects" to be triggered by relatively small changes in the internal or external conditions. Moreover, the non-equilibrium nature of most processes offers a handle for least abundant components to exert switching control over the entire system. Although this may at the same time tackle the kinetic challenge, especially for assemblies of similar and mobile molecules, evolution can more generally be seen to respond by promoting some form of structural order. A prominent example, albeit not the

[1]Leiden Institute of Chemistry, Leiden University, Einsteinweg 55, 2300 RA Leiden, South Holland, the Netherlands

[2]Department of Chemistry and Hylleraas Centre for Quantum Molecular Sciences, P.O.Box 1033, Blindern, Oslo, 0315 Oslo, Norway

[3]Lead contact

*Correspondence: xinmeng.li@kjemi.uio.no (X.L.), a.sevink@chem.leidenuniv.nl (G.J.A.S.)

https://doi.org/10.1016/j.isci.2021.103618

This is an open access article under the CC BY-NC-ND license (http://creativecommons.org/licenses/by-nc-nd/4.0/).

focus of this study, is the distinct partial order that is present in lipid membranes despite the compositional heterogeneity of the constituting lipid mixture. In fact, within this conserved shape, lipid heterogeneity can be seen to provide an additional functional switch for regulating energetic barriers for passive, *i.e.*, not activated by proteins or other factors, transport across membranes via curvature-induced lipid partitioning. For assemblies of constituents that are considerably less mobile than lipids, *e.g.*, large or rigid molecules such as proteins and natural dyes, the same challenges can be met by positioning the system in a section of the phase space where molecules arrange themselves into a metastable framework with crystalline features. Within such a framework, mobility takes the form of conformational dynamics, which includes rotational motions that have been observed for dyes molecules that are structurally programmed for chiral self-assembly (Li et al., 2018,2019).

The positioning of molecular building blocks with approximate lattice regularity is often observed in naturally occurring "soft" assemblies that display an ability to switch. Fibrils assembled from peptide/protein monomers or dimers are abundant in natural systems. These dense assemblies of quite homogeneous composition can be seen to play a key functional role in scaffolding cellular structures and in enabling mechanical work, *e.g.*, the cell cytoskeleton(Wagstaff and Lowe, 2018), myosin filaments (Craig and Woodhead, 2006), bacterial flagella (Imada, 2018), and filamentous bacteriophages (Rakonjac et al., 2011). Other naturally occurring fibrillic assemblies such as amyloids play a role in the development of human disorders (Chiti and Dobson, 2017). While differing in role and precise composition, all such fibrillic assemblies are formed by a nucleated polymerization process, in which a slow spontaneous fibril nucleation step is followed by rapid (a process that is referred to as autocatalytic) growth through elongation and sometimes also bundling into filaments (Saric et al., 2016). Being a responsive structure, growth or shrinkage is further regulated by varying internal and external factors, for instance, via a conformational response to environmental conditions.

A much lesser known but also naturally occurring molecular assembly that combines responsiveness at the semi-classical level with characteristic crystalline features serving energy transport at the mesoscale is the chlorosome, a light-harvesting organelle that forms within the outer lipid envelope of green sulfur bacteria (Pšenčík et al., 2014). These organelles are assembled from hundreds of thousands of various homologs of bacteriochlorophyll (BChl) *c*, *d*, *e*, or *g* pigments and small amounts of carotenoids and quinones. From a functional perspective, chlorosomes can be seen as one of nature's solutions to avoid the rapid quenching of excitonic energy that would take place in an unstructured assembly at this high pigment density. They are designed to couple a significant cross section for incoming light with the ability to transfer exciton energy with high efficiency over distances of several hundreds of nm, enabling green sulfur bacteria to survive in extreme low-light conditions. Like hierarchical fibril-based structures such as fibers and filaments (Coudray et al., 2016; Dauter and Jaskolski, 2018), chlorosomes are hierarchical structures that form via a nucleation and growth process, as bundles of nested cylinders and curved sheets that display ordering on a chiral lattice at a molecular scale (Oostergetel et al., 2010). On the other hand, there are also striking differences with protein-based fibers. Because the predominant components of chlorosomes, essential to the light-harvesting function, are self-assembled BChl pigments, the organelle structure and function are encoded without scaffolding by peptides or proteins. A pseudosymmetric *syn-anti*parallel stacking arrangement of BChls makes that the rigid macrocycles are quasi-regularly stacked with a staggered rotation of the building blocks along the stack (Li et al., 2018). The stacks self-assemble in cylindrical layers that together constitute multilayered concentric tubes, meaning that the curvature of the quasi-2D lattice varies. Reflecting their functional role, which is an optical light-harvesting antenna rather than mechanical scaffolding, the bundle is only loosely packed by an asymmetric membrane composed of galactolipids and proteins that hold the organelle together. The limited complexity renders chlorosomes an important test bed for studying the intricate coupling between electronic, nuclear, and coarser degrees of freedom that are envisioned to be responsible for the efficient transfer of energy in response to excitation.

The chirality that is present in many tubular bioassemblies, see Figure 1, may be seen to directly follow from chirality at the molecular level, and can more generally be considered to originate from a breaking of the symmetry at a basic structural level. This is a universal feature, exemplified by the induced chirality that is observed for helical stacks of bent achiral molecules (Abberley et al., 2018; Salamonczyk et al., 2019). For natural chlorosomes, the helical lattice within the superstructures can be deduced from the diffuse layer lines in the diffraction patterns that are computed from Cryo-EM images (Ganapathy et al., 2009). While the quality of the signal does not allow for the accurate determination of a distinct chiral angle for multistart helices along the stacking direction, it suggests that there is only one angle for the stacks relative to the

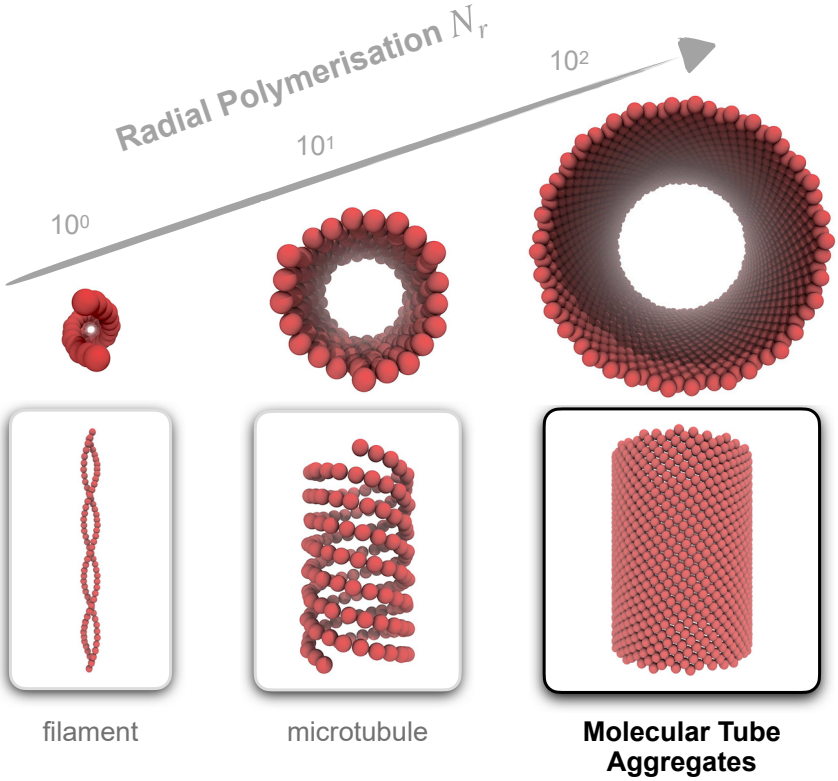

Figure 1. Exemplary members of the class of chiral materials found in biology, ranked by their radial polymerization index N_r

Whereas filaments generally refer to elongated closely packed assemblies of proteins, protein-free molecular tube aggregates assembled from pigments like the chlorosome antenna are also found in nature and exhibit many of the distinct filamentary features. Despite this striking agreement, pigment tubes differ from protein filaments in their (local) molecular degree of freedom, rotational versus conformational, and in the dimensionality of assembly features that emerge from the molecular interaction network, apparent 2D versus 3D, respectively. Figure S1 outlines the chemical structures of composing molecules of chlorosomes and other TMAs. Figure S2 shows the primary rotational motion that exists in the packed pigments of chlorosomes.

tube axis. Circular dichroism (CD) spectra for different organelles show that this angle is sensitive to compositional variations between different types of bacteria and to growth conditions in the same bacteria. *In vitro* reconstitution in a mixture of apolar and polar solvents generally gives rise to tubular or filamentary assemblies that are much larger when compared to the intact chlorosome, with very similar surface charges and optical properties (Kakitani et al., 2007). To understand how to control the helicity, it makes sense to consider how the light-harvesting antenna can be engineered by biological evolution with optimization by natural selection as the main criterion for adaptation to the low-light environment. Based on the observation that the light-harvesting function is conserved across different bacterial species and their mutants featuring different overall chirality, we postulate that their stability during formation is an important control factor for the chirality in chlorosomes. Extracting the relation between chirality and optical and mechanical responses is therefore a primary goal in the current study.

The formation of "soft"' assemblies such as protein fibrils was previously discussed in terms of geometric frustration, which refers to the inability to propagate a preferred pattern of local ordering, for instance, a crystal lattice, into a stable macroscopic assembly with an interface to the environment (Grason, 2016). Especially in systems where weak non-covalent forces hold together rather large, flexible, and chiral molecular building blocks, such an incommensurability between local and global constraints may become tolerated, and defected order can be found to extend over a finite range. Our recent molecular dynamics (MD) studies of model chlorosomes confirmed the stability of regular syn-anti stackings in concentric cylinders for systems composed of pure BChl *c* and *d* and the lack of genuine long-range periodicity observed

in natural and mutant chlorosomes. Moreover, they pointed at the distinct signature of a plastic crystal, a space filling mesophase that is closer to a real solid than, *e.g.*, a liquid crystal. In particular, we found that the weak crystalline positional order is associated with a staggered rotation for each pigment along a distinct dynamic rotational degree of freedom within the confines of the assembly (Li et al., 2018,2019,2020), a feature that is increasingly considered to be essential for their function as an efficient antenna.

While the spatial and temporal resolutions associated with such a motion are typically beyond the experimentally accessible range, Raman spectra for chlorosomes have previously been discussed in terms of modes that directly relate to the interaction network that is responsible for aggregate formation (Cherepy et al., 1996), which agrees well with such rotational motion. The principle rotational (or librational) motions of the BChl head groups, highlighted in the Figure S2 by principal component analysis (PCA), enable us to classify chlorosomes as a plastic molecular crystal (main PCA modes shared in Data S1). Apparently, a transition toward the liquid phase is particularly tuned by nature during evolution, because increased heterogeneity and weakening of the stacking interactions resulting in liquefaction is observed by increased variability in the side chains in the periphery of the pigment macrocycle and substituting small side groups for longer ones (Maruyama et al., 2010). As shown by our MD simulations for BChl assemblies (Li et al., 2018,2019), the transition to a solid or glass phase for decreasing temperature takes the desired form of a damping of the rotational dynamics.

Plastic (molecular) crystals or rotator phases are materials in which molecules only possess a local orientational or conformational freedom of movement. As a transitional stage between real solids and liquids, they offer the option of combining a high enthalpy of transition with a low entropic change, enabling them to reversibly absorb large amounts of heat, which is the reason why such materials have been proposed for thermal energy storage applications (Serrano et al., 2021). Despite the regularity expressed in their molecular packing, which allows them to reach high relative densities, they usually behave like plastic metals under applied mechanical stress, meaning that they, unlike brittle crystalline materials, can be molded into different macroshapes (Das et al., 2020). The originally reported plastic crystals were assembled from small globular molecules that possess a symmetry around the axis of rotation (Chandra et al., 1991).

Our combined findings of weak disorder within each cylindrical layer of the tubular chlorosome, a distinct (2–2.1 nm) inter-cylinder spacing in *silico* and in *vivo* (Ganapathy et al., 2009; Li et al., 2018,2019), indicating that disorder is restricted to within the quasi-2D lattices of varying curvature, and the observation that a flat sheet spontaneously closes up onto itself to form a stable cylinder during 3D molecular simulations *in vacuo*, with BChls displaying a distinct rotational motion within cylinders (Li et al., 2018), provide several strong arguments for classifying chlorosomes as a new type of quasi-2D plastic molecular crystals. Recently, 3D plastic crystal phases that combine distinct positional order with rotational disorder were reported for micrometer-sized charged rod-like colloidal particles that interact through long-ranged repulsion (Liu et al., 2014). Indeed, as discussed by Daan Frenkel (Frenkel, 2015), virtually all phase transitions involving liquids, vapors, crystals, or liquid crystals, even those transitions whose occurrence is commonly attributed to attractive energetic interactions, can be reproduced in colloidal systems where entropy plays a dominant role. In addition, 2D plastic colloidal crystals have been observed upon confinement to a single-layer thin film (Riley and Liddell, 2010; Zhao et al., 2011) and interestingly lack the long-range positional order of their 3D counterparts. The effect of dimensionality on the long-range crystalline order and overall stability of an assembly has been considered theoretically before (Hohenberg, 1967). Following this logic, we may classify fibrillic and filamentary structures based on peptides and proteins, which combine adaptivity through conformational freedom with distinct positional order, as 3D plastic molecular crystals. We believe that this paradigm shift from static structure to responsive function, or equivalently, from stable supramolecular order to restricted dynamic molecular disorder, can be useful for obtaining an improved understanding of their fundamental role as a responsive biomaterial.

Here, we first introduce a protocol for the challenging task of generating an atomically resolved cylindrical plastic crystal structures with user-defined chirality and without steric conflicts in the structure. Plasticity in terms of the local rotational or conformational freedom of movement for constituting molecules is explicitly addressed by the protocol, and an implementation for pigment-based chlorosomes called CTubeGen is made available to the community in order to enable researchers to also study other distinct and attractive mechanical, optical, and other functional properties (Aida et al., 2012; Sengupta and Wurthner, 2013), as

well as the relation between local packing and long-term stability. Implementing the protocol more generally may be useful for the design of artificial systems because large tubular (semi-)synthetic molecular aggregates (TMA) are increasingly considered for electronic and photonic applications (Eisele et al., 2012, 2014; Friedl et al., 2016; Kriete et al., 2017; Matsubara and Tamiaki, 2019; Prokhorov et al., 2015; Short et al., 2013). Considering the molecular building blocks of other TMAs (Herbst et al., 2017; Kriete et al., 2017; Megow et al., 2015; Sengupta and Wurthner, 2013), such as zinc chlorins and amphiphilic cyanine dyes, we may extract design principles for their molecular units, see summary in Figure S1. In general, the quasi-2D structure is stabilized by van der Waals-type of interactions (typically π-π stacking) and electrostatic interactions (typically hydrogen bonding). A typical third element is the tails and sidechains that introduce plasticity and counteract pure crystalline order. The molecular motion in the strong confinement of the assembly is enhanced compared to the dynamics of proteins in a chiral structure, and more relevant for a fast excitonic transfer process. Including the unique role of correlated (classical) vibrations in producing (local) disorder and in driving non-adiabatic quantum-classical transfer is key to the calculation of electronic features, and often disregarded (Li et al., 2020). In addition for realistic *in silico* calculation of other emergent properties, this is a strict requirement (Frederix et al., 2018).

Our second goal of this study is to constitute a direct relation between optical or mechanical properties of chlorosomes and overall chirality, by assembling cylinders at room temperature for equally spaced chiral angles in the full range. To limit the number of computational setups but acknowledge unknown size-dependent factors in natural chlorosomes, which are 100–200 nm in length, 50–100 nm in width, and 15–30 nm in height, we have carefully analyzed the sensitivity of calculated signals to cylinder length and radius in order to select one representative value for each of these variables. Each nested cylinder is constituted by a curved and chiral 2D lattice of pseudosymmetric dimeric unit cells that contain two BChl molecules in a *syn-anti* parallel stacking arrangement (Oostergetel et al., 2010). We show that the calculated optical spectra, *i.e.*, absorption, linear dichroism (LD), and circular dichroism (CD), are sensitive to the chiral angle, and thus provide a fingerprint for determining the chirality of natural and mutant chlorosomes from optical measurements. In particular, our results clarify that seemingly conflicting circular dichroism (CD) signals are consistent with a single chiral angle and explain the uncontrollable variation of optical signatures seen for chlorosomes of the same bacteria (Griebenow et al., 1991; Prokhorenko et al., 2003; Tang et al., 2013). It should be noted that static disorder due to rotational motion has the effect of localizing the excitonic states, but it generally does not change the signature of the absorption, LD, and CD spectra, which are ensemble properties, as discussed in an earlier publication for selected chiral angles (Li et al., 2019,2020). Using a steered molecular approach, we also entered the realm of material science and for the first time considered the relation between chirality and the Young's modulus, quantifying the elastic response to deformation along the cylinder axis. We conclude that also the chlorosome mechanics is sensitive to chirality, rendering it either a relatively soft or hard material, and we link it to the network of interactions. While the stress-strain relation for chlorosomes has not been considered experimentally to our knowledge, they have been imaged using tapping-mode atomic force microscopy (Martinez-Planells et al., 2002). Mechanical stress was applied by the moving AFM tip along the short-axis direction to determine the elastic modulus, *i.e.*, orthogonal to the direction considered in this study, and the self-assembled structure did not disintegrate. Our findings suggest that mechanical stability when the chlorosome is formed within the lipid leaflet may be behind the mysterious selection (or optimization) of a chiral angle, which paves the way for more targeted experimental investigations.

RESULTS AND DISCUSSION

The tube-building protocol

The general protocol for generating atomically resolved tubular structures with a predefined chiral angle is outlined in Figure 2. In the present study, we applied this protocol for generating cylindrical chlorosome tubes composed of *syn-anti* dimeric unit cells of BChl *c*. The basic three steps are further specified:

Stage 1, preparation

The goal of this stage is to generate a proper local packing, by equilibrating small molecular aggregates prior to curving. The molecular basis or composing unit for a given tube system has to be estimated or determined *a priori*. Next, parameters in the force field used for molecular simulation can be selected based on molecular topology and chemistry. This step should be taken with utmost care, as the accuracy of the force field is key to reproducing experimentally observable features. Having selected a proper force field and a unit cell, it is easy to build small quasi-2D assemblies, by multiplying unit cells along the two

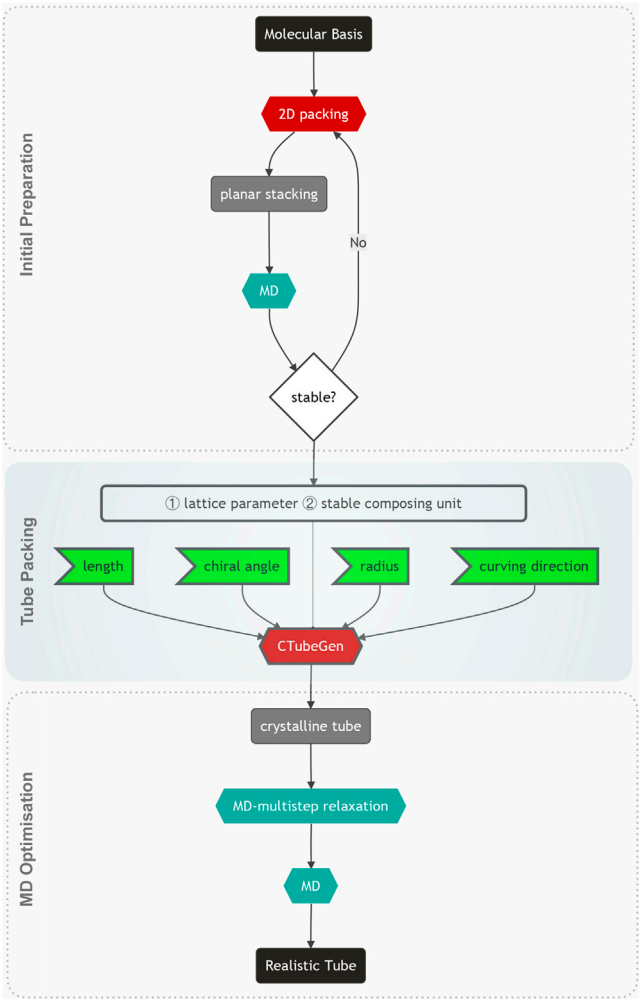

Figure 2. Flowchart for the protocol developed in this study to generate atomistically resolved tube structures

This protocol has been implemented in a computational tool called CTubeGen (see the algorithm details in the STAR method and corresponding pictorial illustration in Figure S3) for the generation of chlorosome tubes with user-defined curving direction, radius, length, and chirality. After an initial preparation stage in which the 2D stacking motif is tested against the considered MD force field, molecules are packed into a tube with preset characteristics during stage 2, and finally, in stage 3, simulated at room temperature to introduce the local disorder and rotational freedom that are also characteristic for 2D plastic crystals.

principal directions of the interaction network that holds the aggregate together. If this aggregate is indeed found to be stable under MD simulation *in vacuo*, meaning that distances and orientations between molecules are conserved, this stage is ready. Concentrating on the BChl assembly in a chlorosome, the composing unit is the *syn-anti* dimeric unit cell that was derived from solid-state nuclear magnetic resonance (NMR) data for chlorosomes and further optimized by DFT calculations (Ganapathy et al., 2009). Using this unit cell and the force field parameterized for BChl molecules (Li et al., 2018), small planar aggregates can be built on a 2D lattice by multiplication along the two-dimensional lattice spanned by the vectors ***a*** and ***b*** (with *a* and *b* representing their length, and γ the angle between them). If this aggregate is found unstable under MD simulation, updated lattice parameters (*a*, *b*, andγ), can either be extracted from the simulated assembly, or they should be tuned prior to simulation until the assembly remains stable. For general cylindrical assemblies, initial values for the parameters (*a*, *b*, andγ) of the underlying Bravais lattice are usually available from the literature, for instance, from crystal diffraction measurements or DFT calculations. If not, one could consider "brute-force" sampling using approximate values for the lattice parameters, knowing that there are only five Bravais lattices in two dimensions.

Stage 2, tube packing

The goal of the second stage is to generate customized tube structures based on the information obtained in the previous stage. Lattice parameters (*a*, *b*, andγ) as well as the unit cell tested in stage 1 form the primary information and are used as input in our packing code. Executing the code without this test may give rise to conflicts at the level of the force field and result in destabilization of preformed aggregates in subsequent MD simulations and/or a mismatch of the overall mass density. The packing code generates molecular tube structures in a highly customizable fashion. User-defined variables include the total length of the tube, the curving direction and tube radius, and the chiral angle. The last two parameters—radius and chiral angle—define the chiral vector relating to the chiral indices (n_1, n_2) as $\boldsymbol{C} = n_1\boldsymbol{a} + n_2\boldsymbol{b}$. A key step in the building process is to convert the supramolecular chirality to a local twist angle α and rise distance *h* needed for the growth of unit cells in a chiral fashion (He and Scheres, 2017; Tsai and Nussinov, 2011). Applying rotation (by an angleα) and translation (over a distance *h*) to a composing unit cell, both along the ***a*** and ***b*** directions and starting from the base of the tube, provides a full tube structure. At this point, it makes sense to identify any molecular overlap in the pre-assembled tube, which can either be done by an internal check or quick visual investigation of the structure. In particular, molecules with a macrocycle may become interlocked upon placement, and such topological issues cannot be resolved by simple relaxation.

Stage 3, MD optimization

The final stage aims at resolving any stress that may result from positioning unit cells onto a very regular tube lattice structure, and on introducing plasticity or structural disorder by MD. To this aim, we perform a set of sequential MD simulations. First, we minimize the energy by steepest descent in order to remove any structural overlap which will cause numerical instability when performing unconstrained MD. Next, we perform MD simulations with a set of positional restraints to resolve frustrations that may cause unfavorable structural defects. In our case, MD simulations with restraints on the head part (or heads) of all molecules aim at relaxing the conformations of the flexible tails. After removing these head restraints, only the positions of the Mg^{2+} ions are restrained, allowing all other atoms in the head part to relax while keeping the lattice of unit cells fixed on a higher structural level. After this step, all position restraints are removed, and we perform mild thermal annealing by unconstrained MD at a reduced temperature of 50 K. Finally, the structure is sufficiently equilibrated to perform unconstrained MD simulations in the target thermodynamic conditions, which, in our case, are at room temperature. We note that it is also possible to include solvent at this stage, in order to study tube structures beyond the *in vacuo* conditions. If so, it is sensible to optimize the unit cell via MD simulation of planar aggregates in the preferred solvent at stage 1.

An entire family of chlorosomal tubes

Disregarding the direction in which the lattice is curved, tube chirality is uniquely defined by the chiral angle δ, which is defined as the angle between the rolling vector and a reference lattice vector, in our case ***a***, see Figure 3A. To systematically study the role of chirality, we used the protocol to assemble tubes in the full chiral angle range $\delta \in [0°, 180°]$ with a resolution of 5° (results for $\delta \in [180°, 360°]$ follow from symmetry considerations). We focus on a curving direction that is consistent with the one identified for all spontaneously formed cylindrical assemblies (Li et al., 2018), with *syn* tails always positioned at the inner side of the tube.

From a conceptual viewpoint, it is important to note that emergent properties are often determined by much coarser features of biomaterials than those represented at the atomic (or even finer) resolution. Consequently, one may conclude that ensemble properties may well be only indirectly sensitive to the more resolved chemical detail. For instance, the electronic response to excitation, which gives rise to the calculated optical responses that favorably compare to measured spectra, is described by the only treatment that can deal with such huge assemblies, and as such fully parametrized by features at the molecular and supramolecular level (derived from induced molecular dipoles and the local excitation energy) (Li et al., 2019,2020). While this aligns well with the essentially linear nature of human perception, *i.e.*, tiny perturbations constitute a tiny effect in the observable, this conflicts with the idea of biological triggering. Indeed, MD simulations have shown that mixing in tiny amounts of BChl *d*, which differ from the BChl *c* matrix in only one side group, constitutes a much stronger perturbation of the spontaneously formed chirality than one would expect based on a linear relation (unpublished data). Although we thus have to keep in mind that chirality is sensitive to such detail, the good news is that the determined relation between chirality and emergent optical properties is not, so we may generalize it to other BChl pigments and/or BChl mixtures.

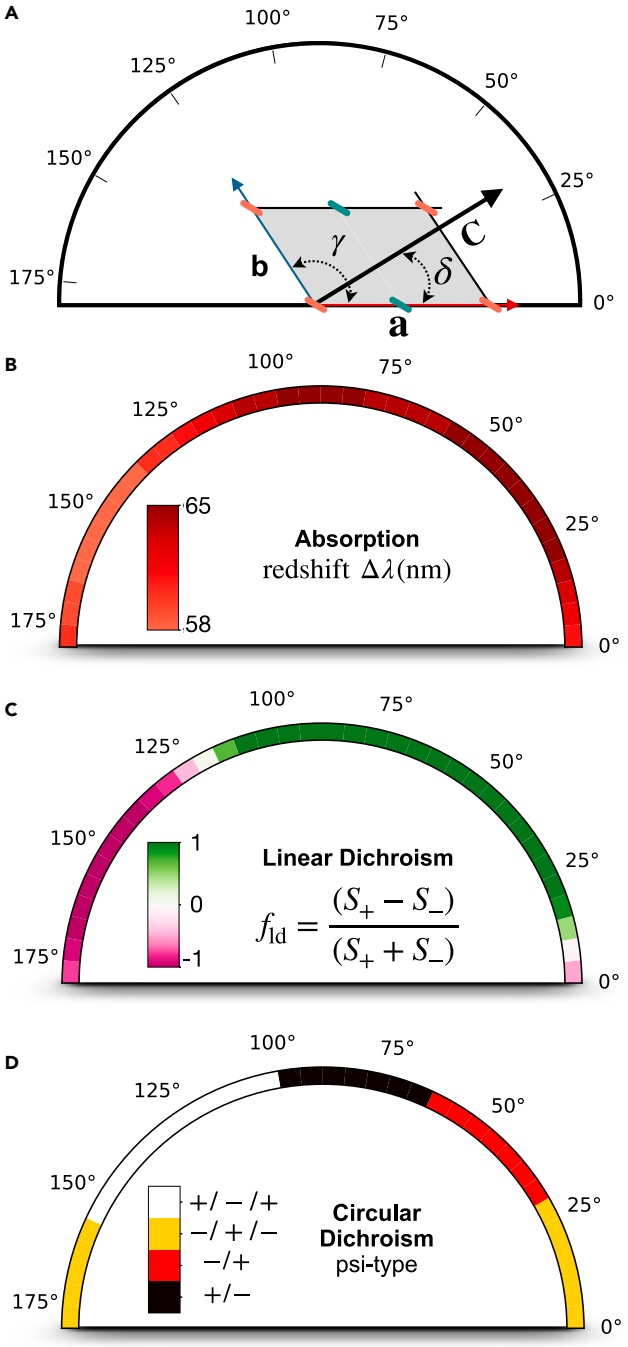

Figure 3. Optical spectra dependence on tube chirality

(A) Schematics of the 2D helical lattice composed of *syn-anti* packing units and the chiral angle δ. The polar axis is defined according toδ.

(B–D) Polar plot of spectral features for absorption (B), LD (C), and CD (D) as a function of δ. The resolution for δ is 5°. For all considered δ tube structures, spectral signatures are identified from spectra that were broadened using a Gaussian kernel with FWHM equal to 200 cm^{-1}, see all the plots in supplemental information (Data S2).

We pre-assembled tubes of BChl *c* with dimensions that are comparable to those of actual chlorosomes to avoid uncertainty about the relevance of our computational results for experimental systems. Owing to the 2D nature of tubes, the tube diameter is not a very relevant parameter, and we selected a realistic 15 nm. Theoretical and computational studies indicate that calculated optical spectra are, however, sensitive to the length of the tube,

in particular the signature of the CD spectra, which can vary with length for a fixed δ (Prokhorenko et al., 2003; Tang et al., 2013). Because we observed no signature change of calculated CD spectra for lengths exceeding 60 nm (Li et al., 2019), we have considered 60 nm tubes in our systematic analysis. For each chiral angle, a tube composed of roughly half a million atoms was positioned in the center of a sufficiently large simulation volume in order to avoid interactions with periodic images. In the stage of unrestrained MD simulations, tube structures were simulated for 5 ns at 50 K and sequentially another 5 ns at 300 K.

Our results show that chirality is only a very minor factor in the structural stability, as exemplified by the stability observed for pre-assembled tubes in the full range of chiral angles over 10 ns of MD simulation. This is consistent with entropy providing only a weak driving force for the (re)assembly of hierarchical structures. Moreover, we found that disorder in the form of rotations of individual molecules is present in all considered closely packed tubes, albeit with δ-dependent rotational angle distributions, very similar to the rotational degree of freedom that we previously identified in single curved sheet (Li et al., 2018). This led us to the conclusion that the dynamic heterogeneity is rather indifferent to the overall tube chirality δ.

Of course, this conclusion is only strictly valid for the considered tube radius. To evaluate the effect of different curvature on chirality-dependent properties, one may consider $|n_1| + |n_2|$as an additional variable that sets the radius of the cylinder. In our setup, chosen to represent a quasi-2D sheet in a tubular chlorosome, $|n_1| + |n_2|$ is relatively large, or the local curvature small, and the local packing environment for the composing unit is similar to that of the planar situation. In other words, the quasi-2D interaction network between composing pigments is only mildly deformed when curved. While cryo-EM images of natural chlorosomes show curved partial sheets to coexist with full tubular multilayered structures, suggesting that the effect of curvature on pigment packing within sheets is indeed fairly limited, it may well explain why a central cylinder is always missing in natural tubular chlorosomes (Ganapathy et al., 2009). Moreover, optical spectra obtained from isolated chlorosomes strongly suggest that chirality is conserved among the individual cylindrical layers of the multilayered assembly (Gunther et al., 2016; Günther et al., 2018). Finally, for the tiny $|n_1| + |n_2|$ in protein filaments and microtubules, which can be seen equivalent to the missing central cylinder in a chlorosome, frustration due to the packing of 2D unit cells into a strongly curved chiral structure would be substantial. This reflects once more the genuine 3D nature of such filaments.

Chirality-dependent properties

Optical properties

We have used the cylindrical structures generated by our protocol for the full range of chiral angles to calculate absorption, LD, and CD spectra. Spectra were determined via a Frenkel exciton Hamiltonian, in which electronic couplings between pigments only depend on the distance and relative orientations between molecular transition dipoles, see more discussions in our previous work (Li et al., 2019). A common procedure for broadening the calculated stick spectra, via a convolution with a Gaussian of varying width, was applied to mimic experimental broadening due to heterogeneity and radial variations in experimental assemblies. To provide insight into the effect that this broadening has on the spectra, we show spectra for Gaussian filters with FWHM values ranging from 10 to 350 cm^{-1} (see all spectral plots in the Data S2).

We have used two scalar measures to characterize the spectral features (Li et al., 2019). The absorption spectrum is characterized by the redshift $\Delta\lambda = \lambda_m - \lambda_0$, with $\lambda_m$the position of the brightest absorption peak and λ_0 the excitation energy of a monomer, and the LD spectra by $f_{ld} = (S_+ - S_-)/(S_+ + S_-)$. Here, S_+ and S_- are the integrated areas of the positive and negative bands of the LD spectrum, respectively. Positive or negative f_{ld} discriminates between structures that possess a stronger or weaker absorption along the tube axis than that orthogonal to the tube axis, respectively. CD spectra are only characterized by the type of the psi-shapes, of which there are four different options: $-/+$, $+/-$, $-/+/-$, $+/-/+$ (Li et al., 2019).

Figure 3 illustrates spectral features in terms of these characteristics for the full range of chiral angles δ. It enables us to group structures into categories with equivalent optical properties. Clearly, the sensitivity of the optical spectra to supramolecular chirality is less for absorption than for LD, and for LD it is smaller than for CD, which is the most sensitive. For absorption, see Figure 3B, a very constant redshift $\Delta\lambda \approx 60\ nm$ can be seen for all δ, which simply demonstrates that indeed all tubes belong to the class of J-aggregates (Eisfeld and Briggs, 2006). This is consistent with earlier findings that the local *syn-anti* pigment packing determines the Q_y absorption band rather than chirality on a higher structural level. For LD and CD, the role of

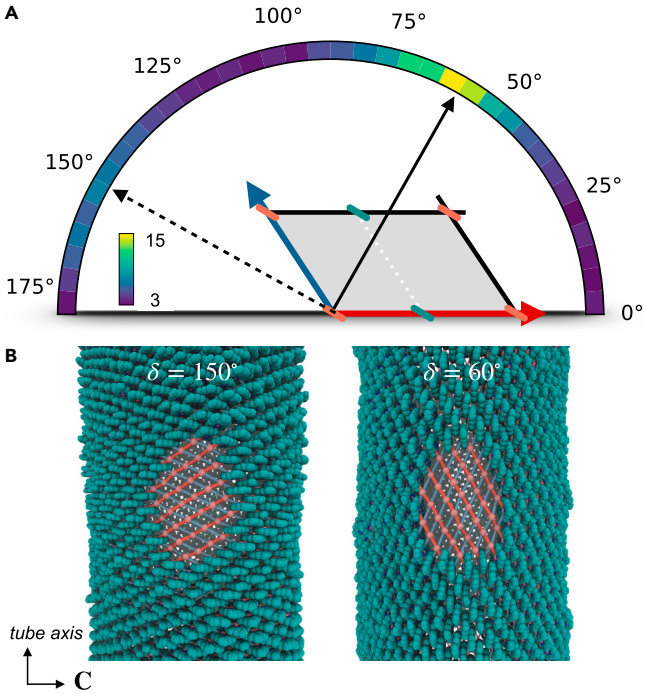

Figure 4. Axial compression modulus dependence on tube chirality

(A) Polar plot of the axial (compression) modulus Υ as a function of the chiral angle δ (numerical values listed in Table S1, see simulation details in the STAR method and corresponding illustration in Figure S4). As before, the resolution for δ is 5°.

(B) Snapshots of BChl *c* assemblies for $\delta_1 = 60°$ and $\delta_2 = 150° = \delta_1 + 90°$ associated with the two maxima of the modulus Υ. In a small round section of the tube, molecules are represented only by their Mg^{2+} ion in order to clarify the chiral nature of their packing.

this chirality is more relevant. For LD, see Figure 3C, the changing sign of f_{ld} divides the δ range into *three* distinct domains: upon increasing δ from 0° to 175°, f_{ld} changes from negative to positive, and then to negative again. Because $f_{ld} \approx 1$ for all measured LD spectra, we conclude that $\delta \in [15°, 110°]$ is consistent with experimental characterization. At the same time, it confirms the very recent conclusion that LD alone is insufficient to determine a particular value (Günther et al., 2021). As shown in Figure 3D, the CD spectrum is most sensitive to the chirality and *five* distinct domains can be identified. Our results show that mixed-type CD spectra, for instance, the $-/+/-$ type frequently observed for natural chlorosomes, are consistent with a single tube, and serve as further proof for the probability of a common chirality that stems from externally applied conditions on the entire chlorosome. In particular, it shows that a mixed signal does not necessitate mixing of optical signals in a superstructure that contains elements with opposing chirality, as has been suggested in the literature (Griebenow et al., 1991). The different types of CD spectra observed experimentally for the same chlorosomes can now be explained more quantitatively by the observation that the structure of chlorosomes is known to depend on specific growth conditions. For instance, going from 25° to 30°, the psi-type CD signal changes from $-/+/-$ to $-/+$. Finally, we note that reversing the curving direction will reverse the tube chirality (Li et al., 2019). It will simply switch the sign of CD spectra and has little effect on the absorption and LD spectra.

Mechanical properties

To quantify the relation between chirality and emergent mechanical properties, we also conducted steered molecular dynamics simulations upon all considered chlorosomal tubes. The computational procedure was previously applied for determining linear stress-strain relations for protein filaments and is outlined in more detail in STAR method and Figure S4. It follows the standard form of computationally measuring the force-deformation relation upon pulling or pushing part of the (fixed) structure by attaching a harmonic spring that moves with constant velocity, followed by extracting the axial (compression) modulus Υ from the linear part of this relation, see Figures 4A and S4. Because we push along the tube axis, this Υ can be seen to correspond to Young's modulus due to compression.

The Young's modulus is indeed found to vary substantially with the chiral angle δ. As comparison, extremes determined for our tubular assemblies relate to "soft" materials like collagen fibers (3 GPa) and "hard" human cortical bone (15 GPa) (Chen et al., 2008). The deformation (or, equivalently, the force) associated with a crossover to a nonlinear stress-strain regime, denoting the onset of tube buckling, is found inversely correlated with the Young's modulus, as expected, signaling that pigments in tubes associated with a high Young's modulus are more likely to disassemble from their weak crystalline arrangement when force or pressure is applied. During formation, when the assembly grows in a lens-like inclusion and a parallel orientation to the surrounding lipid membrane, the principal component of the force exerted on the tubes will indeed be along this tube axis. The relative softness that is observed in part of the δ range explains the resilience to such an applied force, especially when taken into account that chlorosomes already live in a high-pressure environment, *i.e.*, deep sea where the green sulfur bacteria can be found, which may translate into local conditions. In Figure S5, we additionally show Υ along with the maximum deformation, which is defined as ΔL for which the linear relation between force and deformation starts to break down. Beyond this deformation or force, the tube starts to buckle. As expected, the axial modulus is anti-correlated with this maximal deformation, meaning that deformation ΔL to which cylinders are able to respond elastically grows with decreasing modulusΥ.

Analyzing the angle-dependent Young's moduli, see Table S1, we find the peak value associated with the hardest material for $\delta_1 = 60°$ (Υ= 14.1 Gpa), with another peak of half this size at $\delta_2 = 150°$ (Υ= 7.0 Gpa). In Figure 4A, these two particular δ values are labeled by solid and dashed arrows, respectively. The softest materials, on the other hand, are associated with minima in the two valleys between these peaks, with the deepest one located around the global minimum $\delta = 20°$ with Υ= 3.4 Gpa. It is promising to see that this chiral angle indeed agrees remarkably well with at least one of the angles $\delta = 19.8°$ and 27.6° that are consistent with the experimental layer line positions and optical signatures for chlorosomes of bchQRU mutants that are rich in BChl *d* (Li et al., 2019). On the other hand, the two consistent chiral angles $\delta = 42.3°$ and 49.6° for wild-type (WT) chlorosomes (Li et al., 2019), which are rich in BChl *c*, give rise to rather hard materials. Yet, for a reversed curving direction and $\delta = 112.3^*$, where the asterix signals the reversed curving, consistency (apart from the LD spectra) is again combined with considerable softness. To constitute a proper match for all experimental signatures, we did previously identify a slightly smaller angle $\delta = 105^*$ (with Young's modulus Υ= 3.8 Gpa) that is consistent if we take the tiny margins into account that were found for the lattice parameters in step 1 of the protocol (Li et al., 2019). The finding of a transition between the $(-/+/-)$ type ($\delta = 112.3^*$) and the $(-/+)$ type ($\delta = 105^*$) CD spectra, see Figure 3, now helps us to further explain how these two different CD spectra can be measured for one type of WT chlorosomes (Griebenow et al., 1991; Tang et al., 2013). In particular, one should realize that such a tiny perturbation could be induced by traces of other BChls in WT chlorosomes, especially when the trace amounts can slightly vary between very similar organelles (unpublished data). With this note, we will focus on $\delta = 112.3^*$ as representative for the WT chlorosome in the remainder. The softness in the local minimum is indeed very comparable to the one in the global minimum. Combining the mechanical properties with structural information considered in our earlier studies, see the Figure S6 for an overview, we arrive at distinct chirality: wild-type chlorosomes assembled from BChl *c* feature a chiral angle $\delta = 112.3^*$,while BChl *d*-based chlorosomes of bchQRU mutants feature a chiral angle $\delta = 20°$. For completeness and future usage, pdb structure files for the two cases are supplemented in the supplemental information as well (Data S3 and S4). Yet, the observation that complimentary experimental characterization methods never considered chlorosomes grown under exactly the same conditions remains a source of uncertainty. As illustrated and discussed throughout this study, the librational motion of dyes within a structured high-density assembly is the actual key feature that is conserved in all chlorosomes, while chirality is obviously rather an exclusive than a determinative property for both function and stability.

One may intuitively relate the mechanical response of the material to the deformation of the complex network of (non-bonded) interactions between constituent molecules. In particular, chlorosomes will behave as a relatively "soft" material if the constituting pigments are able to slide along each other upon applying an external force without significantly perturbing this interaction network. Examining the molecular configurations of the two δ associated with largest Young's moduli, see snapshots in Figure 4B, we found that they indeed correspond to very particular deformations. The first one, $\delta_1 = 60°$, corresponds to the situation that the hydrogen bonds between BChl molecules align with the direction in which the force is applied (along the tube axis). Thus, like in other biological systems, hydrogen bonding plays a vital role in the mechanical properties (or, more strictly, the axial modulus). We note that hydrogen bonds were

previously already identified as a key structural element for the rotational dynamics (Li et al., 2018). The second situation, $\delta_2 = 150° = \delta_1 + 90°$, corresponds to the composing BChl molecules aligning perpendicular to the tube axis. In this situation, the maximum compression is along the π-π stacking interaction network between neighboring BChl macrocycles. The associated Young's modulus corroborates that deformation of the π-π stacking interaction network has indeed a less significant effect on the elasticity when compared with hydrogen bonding.

While the hardest material can thus simply be deduced from knowledge of the particular network of non-bonded interactions that stabilize the assembly, our steered MD procedure does provide new quantitative information into the role of external factors for varying chirality. While this information is not directly revealed in experiments, which measure either the flexural rigidity or the response to radial deformation, it helps in understanding the conditions during nucleation and growth of pigment assemblies and in further narrowing down the chirality associated with natural or mutant chlorosomes. More generally, this work demonstrates the possibility of combining different levels of structural information to produce all-atom models that are suitable for quantitative analysis of structure and structural responses, which extends the range of systems amenable to *in silico* study and should enable exciting advances in our microscopic knowledge of biology (Wells and Aksimentiev, 2010).

Benefits of plastic crystal feature

Most often light-harvesting antennae in nature take the form of pigment-protein complexes, in which proteins provide structural support for the pigments. In comparison, pigments in chlorosomes generate their own scaffolding. By abandoning the protein matrix, pigments can self-assemble in a huge structure at an impressive pigment concentration, estimated to be 1∼2 mol/L. In chlorosomes, the competing process of excited-state quenching is overcome by ultrafast delocalization and transfer into the photosynthetic conversion chain. This strategy is needed to enhance the capability of capturing photons and allows the bacteria to survive in low-light conditions. The key element in this strategy is the plastic crystal feature, which enables chlorosomes to adopt the specific energy transfer mechanism of *supertransfer* (Kassal et al., 2013).

The intrinsic heterogeneity of chlorosomes brings along an exciton manifold of only moderately delocalized states that are composed of clusters in size of ten(s) of pigments and *randomly* distributed over the assembly, *i.e.*, generally far-way from the base plate. If the system would only rely on dissipative incoherent energy transfer, sites of low excitonic energy will give rise to a reduced or even detrimental transfer efficiency by trapping and quenching of excitons.

The strategy of chlorosomes to overcome this challenge is to utilize the disorder associated with the thermally induced rotational dynamics, which translates into variations of the excitonic coupling and can change the hydrogen bonding status of BChls, in the plastic crystalline framework for inducing semi-classical transportation of the exciton over the entire self-assembly structure at very short timescales. The nuclear motion in the classical regime prevents the system from settling in quantum eigenstates. The libration of the dipole transition moments induces frequent level crossings in the exciton manifold. Every time a level crossing takes place, its degeneracy will be lifted by the non-adiabatic coupling terms it generates. In this way, thermal motion generates quantum instabilities that continuously disturb the system and create a perpetual random sequence of thermally induced, transient coherences between exciton states. This induced-quantum regime for abundant non-adiabatic conversion by adiabatic passage (NCAP) events between excitonic states represents an efficient machinery for enhancing the exciton dynamics in chlorosomes (Haken and Reineker, 1972; Haken and Strobl, 1973; Huijser et al., 2008; Li et al., 2020). It leads to long-range incoherent transport between clusters of strongly coupled pigments in a supertransfer mechanism, which was indeed observed in our previous work (Li et al., 2020). In particular, the plasticity represented by the thermally driven rotational or librational motions generates a specific type of dynamic disorder that drives the *enhanced sampling* of the exciton over the chlorosome assembly at a short timescale. The timescale is fast enough to help the chlorosomes overcome local trapping in-between photon capturing events and before the exciton annihilates. It also explains why a distinction between homogeneous and inhomogeneous broadening in chlorosomes is not possible (Fetisova and Mauring, 1993; Psencík et al., 1994), since any excitation of one part of the inhomogeneously dispersed exciton manifold of states will homogeneously affect the whole absorption profile because of the delocalization by abundant avoided crossings and transient quantum instabilities induced by the rotational dynamics.

Finally, an important feature of chlorosomes is their tubular geometry. The beauty of the NCAP supertransfer mechanism is that, while evolving toward the low energy side of the exciton band, the exciton is also sampling real space. A tubular geometry increases spatial overlap between exciton states, which will further enhance the sampling and transfer efficiency. The tubular geometry thus follows the general design principle of utilizing the exciton energy in low-light conditions to its maximum.

Conclusions

In this work, we have performed an integrated analysis of chlorosomes from an electronic and materials perspective, by considering the relation between functional (optical) and mechanical properties and large-scale structural characteristics. To enable such an analysis, we set up a general protocol, see Figure 2, for generating atomically resolved tube structures that are found in nature with prescribed tube chirality. The unique element of this protocol is that it deals explicitly with the local molecular degrees of freedom that give rise to classical vibrations and a weakly static disordering of still highly regular molecular packings. We developed and used a particular implementation for chlorosomes, where such vibrations are believed to play a key role in light harvesting. We have determined a systematic relation between two linear responses, optical in terms of the absorption, LD, and CD spectra, and mechanical in terms of the Young's modulus, and the higher order chiral nature of tubular pigment assemblies.

The conceptual significance of this study is the attribution of dense biomolecular assemblies of rather homogeneous composition like chlorosomes to the class of plastic crystals. Albeit mainly of conceptual significance, we believe that such an embedding may turn out very beneficial for future research. Working on shared research questions rather than seemingly unrelated issues will increase the applicability of modern hybrid computational treatments that are currently developed for individual members of this class of materials. Moreover, obtaining an improved understanding of how different material aspects combine into particular and robust functions will add to the fundamental insight how nature exploits material characteristics to optimize diverse tasks via specialized structured domains.

Constituting a direct relation between the optical response and chirality (as encoded in the chiral angle δ) generates the first useful map, see Figure 3, for interpreting optical spectra that have been measured for chlorosomes. Incorporating further improvements is straightforward, for instance, in the accuracy of the MD force field or the electronic coupling used to construct a Frenkel Hamiltonian. For the determination of the mechanical responses under axial compression for varying δ, which to our knowledge has not been considered for chlorosomes before, we have used the same steered molecular dynamics treatment that was previously employed for protein filaments to generate a map, see Figure 4. Our results indicate that, despite their optical function, "softness" or resilience to compression is indeed the key factor in the selection of a particular chirality.

Combining all available information—scattering, optics, and mechanics—we confirm that nature is flexible in linking mild compositional and structural diversity with functional robustness in bacterial light harvesting. We have identified that wild-type chlorosomes assembled from BChl *c* feature a chiral angle $\delta = 112^{\circ}$ and curve with the *anti* tails positioned at the inner side of the tube. On the other hand, BChl *d*-based chlorosomes of bchQRU mutants feature a chiral angle $\delta = 20^{\circ}$ and curve in the opposite direction, with *syn* tails positioned at the inner side of the tube. Interestingly, our finding that nature is able to structurally diverge to secure the same optical function, a response that can tolerate or even relies on mild structural disorder, clarifies why optical data alone are insufficient for solving the inverse problem. Experimental testing of the role of the mechanics in the selection of chirality will thus resolve this long-standing issue in chlorosome research and is likely to enable better control and manipulation of entire natural and synthetic organelles for the first time. Finally, we mention that our treatment is transferable to other large-scale optically or mechanically responsive molecular aggregates of technological or biological relevance, such as optically active designer nanomaterials, protein filaments, and microtubules.

Limitations of the study

There are limitations for this study. Experimental characterization of the motion of individual molecules in a large aggregate at a nanosecond timescale is a major challenge and will remain so for some time, so momentarily we rely on indirect experimental evidence (Raman spectra, diffuse scattering patterns, localization of excitonic states, etc.) for the molecular motion observed in our MD simulations. While measuring the mechanical response of individual chlorosomes can provide further insight into such degrees of

freedom, as molecules in our steered MD are seen to respond to tube deformation by rotation, the setup for determining such a response in chlorosomes, e.g., via atomic force microscopy, presents practical challenges. How the lipidic surroundings for the pigment assembly during chlorosomes growth in green sulfur bacteria influences the growth process, and how it relates to growth in a solvent-rich environment, is experimentally inaccessible. In particular, chlorosomes reconstitution in a mixture of polar and apolar solvents gives rise to visually and functionally related aggregates, but their fine structure remains beyond resolution. On the methodological side, our MD force field can be further refined to better capture intramolecular breathing modes of the macrocycle. Simulations of tubular assemblies have been carried out in vacuo for reasons of computational feasibility. While solvent-mediated effects are expected to be minor, they are not captured in our setup.

STAR★METHODS

Detailed methods are provided in the online version of this paper and include the following:

- KEY RESOURCES TABLE
- RESOURCE AVAILABILITY
  - Lead contact
  - Materials availability
  - Data and code availability
- METHOD DETAILS
  - The algorithm of the tube packing code CTubeGen
  - Molecular dynamics simulations
  - Optical spectra calculation
  - Simulation of mechanical properties

SUPPLEMENTAL INFORMATION

Supplemental information can be found online at https://doi.org/10.1016/j.isci.2021.103618.

ACKNOWLEDGMENTS

The use of supercomputer facilities at SurfSara was sponsored by NWO Exact and Natural Sciences, with financial support from the Netherlands Organization for Scientific Research (NWO). X.L. acknowledges the support of the Norwegian Research Council through the CoE Hylleraas Center for Quantum Molecular Sciences (Grant No. 262695).

AUTHOR CONTRIBUTIONS

X.L. and G.J.A.S. conceived the research; X.L carried out the simulations and analyzed results; X.L. and G.J.A.S. prepared the manuscript with input from all authors. All the authors contributed to the scientific discussion and in editing the manuscript.

DECLARATION OF INTERESTS

The authors declare no competing interests.

Received: August 17, 2021
Revised: November 15, 2021
Accepted: December 8, 2021
Published: January 21, 2022

REFERENCES

Abberley, J.P., Killah, R., Walker, R., Storey, J.M.D., Imrie, C.T., Salamonczyk, M., Zhu, C.H., Gorecka, E., and Pociecha, D. (2018). Heliconical smectic phases formed by achiral molecules. Nat. Commun. *9*, 228. https://doi.org/10.1038/s41467-017-02626-6.

Abraham, M.J., Murtola, T., Schulz, R., Páll, S., Smith, J.C., Hess, B., and Lindahl, E. (2015). GROMACS: high performance molecular simulations through multi-level parallelism from laptops to supercomputers. SoftwareX *1-2*, 19–25. https://doi.org/10.1016/j.softx.2015.06.001.

Aida, T., Meijer, E.W., and Stupp, S.I. (2012). Functional supramolecular polymers. Science *335*, 813–817. https://doi.org/10.1126/science.1205962.

Badeau, B.A., and DeForest, C.A. (2019). Programming stimuli-responsive behavior into biomaterials. In Annual Review of Biomedical Engineering, *Vol 21*, M.L. Yamush, ed., pp. 241–265. https://doi.org/10.1146/annurev-bioeng-060418-052324.

Bussi, G., Donadio, D., and Parrinello, M. (2007). Canonical sampling through velocity rescaling. J. Chem. Phys. *126*, 014101. https://doi.org/10.1063/1.2408420.

Chandra, D., Ding, W., Lynch, R.A., and Tomilinson, J.J. (1991). Phase-transitions in plastic crystals. J. Less-Common Met. *168*, 159–167. https://doi.org/10.1016/0022-5088(91)90042-3.

Chen, P.Y., Lin, A.Y.M., Lin, Y.S., Seki, Y., Stokes, A.G., Peyras, J., Olevsky, E.A., Meyers, M.A., and McKittrick, J. (2008). Structure and mechanical properties of selected biological materials. J. Mech. Behav. Biomed. Mater. *1*, 208–226. https://doi.org/10.1016/j.jmbbm.2008.02.003.

Cherepy, N.J., Du, M., Holzwarth, A.R., and Mathies, R.A. (1996). Near-infrared resonance Raman spectra of chlorosomes: probing nuclear coupling in electronic energy transfer. J. Phys. Chem. *100*, 4662–4671. https://doi.org/10.1021/jp952992e.

Chiti, F., and Dobson, C.M. (2017). Protein misfolding, amyloid formation, and human disease: a summary of progress over the last decade. In Annual Review of Biochemistry, *Vol 86*, R.D. Kornberg, ed., pp. 27–68. https://doi.org/10.1146/annurev-biochem-061516-045115.

Cornell, W.D., Cieplak, P., Bayly, C.I., and Kollman, P.A. (1993). Application of RESP charges to calculate conformational energies, hydrogen bond energies, and free energies of solvation. J. Am. Chem. Soc. *115*, 9620–9631. https://doi.org/10.1021/ja00074a030.

Coudray, N., Lasala, R., Zhang, Z.N., Clark, K.M., Dumont, M.E., and Stokes, D.L. (2016). Deducing the symmetry of helical assemblies: applications to membrane proteins. J. Struct. Biol. *195*, 167–178. https://doi.org/10.1016/j.jsb.2016.05.011.

Craig, R., and Woodhead, J.L. (2006). Structure and function of myosin filaments. Curr. Opin. Struct. Biol. *16*, 204–212. https://doi.org/10.1016/j.sbi.2006.03.006.

Das, S., Mondal, A., and Reddy, C.M. (2020). Harnessing molecular rotations in plastic crystals: a holistic view for crystal engineering of adaptive soft materials. Chem. Soc. Rev. *49*, 8878–8896. https://doi.org/10.1039/d0cs00475h.

Dauter, Z., and Jaskolski, M. (2018). On the helical arrangements of protein molecules. Protein Sci. *27*, 643–652. https://doi.org/10.1002/pro.3356.

Egan, P., Sinko, R., LeDuc, P.R., and Keten, S. (2015). The role of mechanics in biological and bio-inspired systems. Nat. Commun. *6*, 7418. https://doi.org/10.1038/ncomms8418.

Eisele, D.M., Cone, C.W., Bloemsma, E.A., Vlaming, S.M., van der Kwaak, C.G.F., Silbey, R.J., Bawendi, M.G., Knoester, J., Rabe, J.P., and Vanden Bout, D.A. (2012). Utilizing redox-chemistry to elucidate the nature of exciton transitions in supramolecular dye nanotubes. Nat. Chem. *4*, 655–662. https://doi.org/10.1038/nchem.1380.

Eisele, D.M., Arias, D.H., Fu, X.F., Bloemsma, E.A., Steiner, C.P., Jensen, R.A., Rebentrost, P., Eisele, H., Tokmakoff, A., Lloyd, S., et al. (2014). Robust excitons inhabit soft supramolecular nanotubes. Proc. Natl. Acad. Sci. U S A *111*, E3367–E3375. https://doi.org/10.1073/pnas.1408342111.

Eisfeld, A., and Briggs, J.S. (2006). The J- and H-bands of organic dye aggregates. Chem. Phys. *324*, 376–384. https://doi.org/10.1016/j.chemphys.2005.11.015.

Essmann, U., Perera, L., Berkowitz, M.L., Darden, T., Lee, H., and Pedersen, L.G. (1995). A smooth particle mesh Ewald method. J. Chem. Phys. *103*, 8577–8593. https://doi.org/10.1063/1.470117.

Fetisova, Z.G., and Mauring, K. (1993). Spectral hole-burning study of intact-cells of green bacteriumchlorobium-limicola. Febs Lett. *323*, 159–162. https://doi.org/10.1016/0014-5793(93)81470-k.

Frederix, P., Patmanidis, I., and Marrink, S.J. (2018). Molecular simulations of self-assembling bio-inspired supramolecular systems and their connection to experiments. Chem. Soc. Rev. *47*, 3470–3489. https://doi.org/10.1039/c8cs00040a.

Frenkel, D. (2015). Order through entropy. Nat. Mater. *14*, 9–12. https://doi.org/10.1038/nmat4178.

Friedl, C., Renger, T., Berlepsch, H.V., Ludwig, K., Busch, M.S.A., and Megow, J. (2016). Structure prediction of self-assembled dye aggregates from cryogenic transmission electron microscopy, molecular mechanics, and theory of optical spectra. J. Phys. Chem. C *120*, 19416–19433. https://doi.org/10.1021/acs.jpcc.6b05856.

Fujita, T., Brookes, J.C., Saikin, S.K., and Aspuru-Guzik, A. (2012). Memory-assisted exciton diffusion in the chlorosome light-harvesting antenna of green sulfur bacteria. J. Phys. Chem. Lett. *3*, 2357–2361. https://doi.org/10.1021/jz3008326.

Ganapathy, S., Oostergetel, G.T., Wawrzyniak, P.K., Reus, M., Chew, A.G.M., Buda, F., Boekema, E.J., Bryant, D.A., Holzwarth, A.R., and de Groot, H.J.M. (2009). Alternating syn-anti bacteriochlorophylls form concentric helical nanotubes in chlorosomes. Proc. Natl. Acad. Sci. U S A *106*, 8525–8530. https://doi.org/10.1073/pnas.0903534106.

Grason, G.M. (2016). Perspective: geometrically frustrated assemblies. J. Chem. Phys. *145*, 110901. https://doi.org/10.1063/1.4962629.

Griebenow, K., Holzwarth, A.R., Vanmourik, F., and Vangrondelle, R. (1991). Pigment organization and energy transfer in green bacteria. 2. Circular and linear dichroism spectra of protein-containing and protein-free chlorosomes isolated from Chloroflexus aurantiacus strain Ok-70-fl. Biochim. Biophys. Acta *1058*, 194–202. https://doi.org/10.1016/s0005-2728(05)80237-3.

Gunther, L.M., Jendrny, M., Bloemsma, E.A., Tank, M., Oostergetel, G.T., Bryant, D.A., Knoester, J., and Kohler, J. (2016). Structure of light-harvesting aggregates in individual chlorosomes. J. Phys. Chem. B *120*, 5367–5376. https://doi.org/10.1021/acs.jpcb.6b03718.

Günther, L.M., Löhner, A., Reiher, C., Kunsel, T., Jansen, T.L.C., Tank, M., Bryant, D.A., Knoester, J., and Köhler, J. (2018). Structural variations in chlorosomes from wild-type and a bchQR mutant of chlorobaculum tepidum revealed by single-molecule spectroscopy. J. Phys. Chem. B *122*, 6712–6723. https://doi.org/10.1021/acs.jpcb.8b02875.

Günther, L.M., Knoester, J., and Köhler, J. (2021). Limitations of linear dichroism spectroscopy for elucidating structural issues of light-harvesting aggregates in chlorosomes. Molecules *26*, 899.

Haken, H., and Reineker, P. (1972). The coupled coherent and incoherent motion of excitons and its influence on the line shape of optical absorption. Z. für Physik *249*, 253–268. https://doi.org/10.1007/BF01400230.

Haken, H., and Strobl, G. (1973). An exactly solvable model for coherent and incoherent exciton motion. Z. für Physik A Hadrons nuclei *262*, 135–148. https://doi.org/10.1007/BF01399723.

He, S.D., and Scheres, S.H.W. (2017). Helical reconstruction in RELION. J. Struct. Biol. *198*, 163–176. https://doi.org/10.1016/j.jsb.2017.02.003.

Herbst, S., Soberats, B., Leowanawat, P., Lehmann, M., and Wurthner, F. (2017). A columnar liquid-crystal phase formed by hydrogen-bonded perylene bisimide J-aggregates. Angew. Chem. Int. Ed. *56*, 2162–2165. https://doi.org/10.1002/anie.201612047.

Hohenberg, P.C. (1967). Existence of long-range order in one and two dimensions. Phys. Rev. *158*, 383–386. https://doi.org/10.1103/PhysRev.158.383.

Huijser, A., Savenije, T.J., Meskers, S.C.J., Vermeulen, M.J.W., and Siebbeles, L.D.A. (2008). The mechanism of long-range exciton diffusion in a nematically organized porphyrin layer. J. Am. Chem. Soc. *130*, 12496–12500. https://doi.org/10.1021/ja803753y.

Imada, K. (2018). Bacterial flagellar axial structure and its construction. Biophys. Rev. *10*, 559–570. https://doi.org/10.1007/s12551-017-0378-z.

Kakitani, Y., Harada, K.I., Mizoguchi, T., and Koyama, Y. (2007). Isotopic replacement of pigments and a lipid in chlorosomes from Chlorobium limicola: characterization of the resultant chlorosomes. Biochemistry *46*, 6513–6524. https://doi.org/10.1021/bi602586g.

Kaminski, G.A., Friesner, R.A., Tirado-Rives, J., and Jorgensen, W.L. (2001). Evaluation and reparametrization of the OPLS-AA force field for proteins via comparison with accurate quantum chemical calculations on peptides. J. Phys. Chem. B *105*, 6474–6487. https://doi.org/10.1021/jp003919d.

Karki, K., and Roccatano, D. (2011). Molecular dynamics simulation study of chlorophyll a in different organic solvents. J. Chem. Theor. Comput. *7*, 1131–1140. https://doi.org/10.1021/ct1004627.

Kassal, I., Yuen-Zhou, J., and Rahimi-Keshari, S. (2013). Does coherence enhance transport in photosynthesis? J. Phys. Chem. Lett. *4*, 362–367. https://doi.org/10.1021/jz301872b.

Kriete, B., Bondarenko, A.S., Jumde, V.R., Franken, L.E., Minnaard, A.J., Jansen, T.L.C., Knoester, J., and Pshenichnikov, M.S. (2017). Steering self-assembly of amphiphilic molecular

nanostructures via halogen exchange. J. Phys. Chem. Lett. *8*, 2895–2901. https://doi.org/10.1021/acs.jpclett.7b00967.

Li, X., Buda, F., de Groot, H.J.M., and Sevink, G.J.A. (2018). Contrasting modes of self-assembly and hydrogen-bonding heterogeneity in chlorosomes of chlorobaculum tepidum. J. Phys. Chem. C *122*, 14877–14888. https://doi.org/10.1021/acs.jpcc.8b01790.

Li, X., Buda, F., de Groot, H.J.M., and Sevink, G.J.A. (2019). Molecular insight in the optical response of tubular chlorosomal assemblies. J. Phys. Chem. C *123*, 16462–16478. https://doi.org/10.1021/acs.jpcc.9b03913.

Li, X., Buda, F., de Groot, H.J.M., and Sevink, G.J.A. (2020). Dynamic disorder drives exciton transfer in tubular chlorosomal assemblies. J. Phys. Chem. B *124*, 4026–4035. https://doi.org/10.1021/acs.jpcb.0c00441.

Liu, B., Besseling, T.H., Hermes, M., Demirors, A.F., Imhof, A., and van Blaaderen, A. (2014). Switching plastic crystals of colloidal rods with electric fields. Nat. Commun. *5*, 3092. https://doi.org/10.1038/ncomms4092.

Martinez-Planells, A., Arellano, J.B., Borrego, C.A., Lopez-Iglesias, C., Gich, F., and Garcia-Gil, J.S. (2002). Determination of the topography and biometry of chlorosomes by atomic force microscopy. Photosynth. Res. *71*, 83–90. https://doi.org/10.1023/a:1014955614757.

Maruyama, S., Sato, K., and Iwahashi, H. (2010). Room temperature liquid porphyrins. Chem. Lett. *39*, 714–716. https://doi.org/10.1246/cl.2010.714.

Matsubara, S., and Tamiaki, H. (2019). Phototriggered dynamic and biomimetic growth of chlorosomal self-aggregates. J. Am. Chem. Soc. *141*, 1207–1211. https://doi.org/10.1021/jacs.8b13056.

Mattia, E., and Otto, S. (2015). Supramolecular systems chemistry. Nat. Nanotechnol. *10*, 111–119. https://doi.org/10.1038/nnano.2014.337.

Megow, J., Rohr, M.I.S., Busch, M.S.A., Renger, T., Mitric, R., Kirstein, S., Rabe, J.P., and May, V. (2015). Site-dependence of van der Waals interaction explains exciton spectra of double-walled tubular J-aggregates. Phys. Chem. Chem. Phys. *17*, 6741–6747. https://doi.org/10.1039/c4cp05945j.

Oostergetel, G.T., van Amerongen, H., and Boekema, E.J. (2010). The chlorosome: a prototype for efficient light harvesting in photosynthesis. Photosynth. Res. *104*, 245–255. https://doi.org/10.1007/s11120-010-9533-0.

Prokhorenko, V.I., Steensgaard, D.B., and Holzwarth, A.R. (2003). Exciton theory for supramolecular chlorosomal aggregates: 1. Aggregate size dependence of the linear spectra. Biophys. J. *85*, 3173–3186. https://doi.org/10.1016/s0006-3495(03)74735-3.

Prokhorov, V.V., Perelygina, O.M., Pozin, S.I., Mal'tsev, E.I., and Vannikov, A.V. (2015). Polymorphism of two-dimensional cyanine dye J-aggregates and its genesis: fluorescence microscopy and atomic force microscopy study. J. Phys. Chem. B *119*, 15046–15053. https://doi.org/10.1021/acs.jpcb.5b07821.

Psencík, J., Searle, G.F.W., Hála, J., and Schaafsma, T.J. (1994). Fluorescence detected magnetic resonance (FDMR) of green sulfur photosynthetic bacteria Chlorobium sp. Photosynth. Res. *40*, 1–10. https://doi.org/10.1007/BF00019040.

Pšenčík, J., Butcher, S.J., and Tuma, R. (2014). Chlorosomes: structure, function and assembly. In The Structural Basis of Biological Energy Generation, M.F. Hohmann-Marriott, ed. (Springer Netherlands), pp. 77–109. https://doi.org/10.1007/978-94-017-8742-0_5.

Purchase, R., Cogdell, R., Breitling, F., Stadler, V., Hulst, N.v., Kramer, G.J., Ramirez, A., Zwijnenberg, R., Kallergi, A., Baan, J.B.d., et al. (2019). Semi-synthetic responsive matrices for artificial photosynthesis. In Bioinspired Chemistry, K.M. Kadish and R. Guilard, eds. (World Scientific Publishing Co Pte Ltd.), pp. 47–69. https://doi.org/10.1142/9789813274440_0003.

Rakonjac, J., Bennett, N.J., Spagnuolo, J., Gagic, D., and Russel, M. (2011). Filamentous bacteriophage: biology, phage display and nanotechnology applications. Curr. Issues Mol. Biol. *13*, 51–75.

Riley, E.K., and Liddell, C.M. (2010). Confinement-controlled self assembly of colloids with simultaneous isotropic and anisotropic cross-section. Langmuir *26*, 11648–11656. https://doi.org/10.1021/la100361y.

Romero, E., Augulis, R., Novoderezhkin, V.I., Ferretti, M., Thieme, J., Zigmantas, D., and van Grondelle, R. (2014). Quantum coherence in photosynthesis for efficient solar-energy conversion. Nat. Phys. *10*, 677–683. https://doi.org/10.1038/nphys3017.

Saikin, S.K., Eisfeld, A., Valleau, S., and Aspuru-Guzik, A. (2013). Photonics meets excitonics: natural and artificial molecular aggregates. Nanophotonics *2*, 21–38. https://doi.org/10.1515/nanoph-2012-0025.

Salamonczyk, M., Vaupotic, N., Pociecha, D., Walker, R., Storey, J.M.D., Imrie, C.T., Wang, C., Zhu, C.H., and Gorecka, E. (2019). Multi-level chirality in liquid crystals formed by achiral molecules. Nat. Commun. *10*, 1922. https://doi.org/10.1038/s41467-019-09862-y.

Saric, A., Michaelsa, T.C.T., Zaccone, A., Knowles, T.P.J., and Frenkel, D. (2016). Kinetics of spontaneous filament nucleation via oligomers: insights from theory and simulation. J. Chem. Phys. *145*, 211926. https://doi.org/10.1063/1.4965040.

Scholes, G.D., Fleming, G.R., Chen, L.X., Aspuru-Guzik, A., Buchleitner, A., Coker, D.F., Engel, G.S., van Grondelle, R., Ishizaki, A., Jonas, D.M., et al. (2017). Using coherence to enhance function in chemical and biophysical systems. Nature *543*, 647–656. https://doi.org/10.1038/nature21425.

Sengupta, S., and Wurthner, F. (2013). Chlorophyll J-aggregates: from bioinspired dye stacks to nanotubes, liquid crystals, and biosupramolecular electronics. Acc. Chem. Res. *46*, 2498–2512. https://doi.org/10.1021/ar400017u.

Serrano, A., Duran, M., Dauvergne, J.L., Doppiu, S., and Del Barrio, E.P. (2021). Tailored transition temperature plastic crystals with enhanced thermal energy storage capacity. Solar Energy Mater. Solar Cells *220*, 110848. https://doi.org/10.1016/j.solmat.2020.110848.

Short, J.M., Berriman, J.A., Kubel, C., El-Hachemi, Z., Naubron, J.V., and Balaban, T.S. (2013). Electron cryo-microscopy of TPPS4 center dot 2HCl tubes reveals a helical organisation explaining the origin of their chirality. Chemphyschem *14*, 3209–3214. https://doi.org/10.1002/cphc.201300606.

Stingaciu, L.R., O'Neill, H., Liberton, M., Urban, V.S., Pakrasi, H.B., and Ohl, M. (2016). Revealing the dynamics of thylakoid membranes in living cyanobacterial cells. Sci. Rep. *6*, 19627. https://doi.org/10.1038/srep19627.

Tang, J.K.H., Saikin, S.K., Pingali, S.V., Enriquez, M.M., Huh, J., Frank, H.A., Urban, V.S., and Aspuru-Guzik, A. (2013). Temperature and carbon assimilation regulate the chlorosome biogenesis in green sulfur bacteria. Biophys. J. *105*, 1346–1356. https://doi.org/10.1016/j.bpj.2013.07.027.

Tsai, C.J., and Nussinov, R. (2011). A unified convention for biological assemblies with helical symmetry. Acta Crystallogr. Sect. DBiol. Crystallogr. *67*, 716–728. https://doi.org/10.1107/s0907444911024024.

Wagstaff, J., and Lowe, J. (2018). Prokaryotic cytoskeletons: protein filaments organizing small cells. Nat. Rev. Microbiol. *16*, 187–201. https://doi.org/10.1038/nrmicro.2017.153.

Wells, D.B., and Aksimentiev, A. (2010). Mechanical properties of a complete microtubule revealed through molecular dynamics simulation. Biophys. J. *99*, 629–637. https://doi.org/10.1016/j.bpj.2010.04.038.

Zhao, K., Bruinsma, R., and Mason, T.G. (2011). Entropic crystal-crystal transitions of Brownian squares. Proc. Natl. Acad. Sci. U S A *108*, 2684–2687. https://doi.org/10.1073/pnas.1014942108.

STAR★METHODS

KEY RESOURCES TABLE

REAGENT or RESOURCE	SOURCE	IDENTIFIER
Software and algorithms		
Gromacs	Abraham et al. (2015)	http://www.gromacs.org/
Tube packing code CTubeGen	This paper; Zenodo repository	https://doi.org/10.5281/zenodo.3677028

RESOURCE AVAILABILITY

Lead contact

Further information and requests for resources should be directed to and will be fulfilled by the lead contact, G. J. Agur. Sevink (a.sevink@chem.leidenuniv.nl).

Materials availability

No materials were used in this study.

Data and code availability

- All the atomistic tube structure data have been deposited at Zenodo and are publicly available (Zenodo: https://doi.org/10.5281/zenodo.4603352). All relevant data are available from the lead contact upon reasonable request.
- The tube packing code has been deposited at Zenodo and is publicly available as of the date of publication. The DOI is listed in the key resources table.
- Any additional information required to reanalyze the data reported in this paper is available from the lead contact upon request.

METHOD DETAILS

The algorithm of the tube packing code CTubeGen

Step 1. Determination of chiral lattice and helix growth parameters. We define the following pre-requisites:

- Select lattice parameters ($|\boldsymbol{a}| = a$, $|\boldsymbol{b}| = b$, γ) for the unit cell. For BChl *c*chlorosomes: $a = 1.48$ nm, $b = 0.98$ nm, $\gamma = 124.3°$ (Li et al., 2018).
- A regular lattice on the tube can only be formed with a rolling or chiral vector $|\boldsymbol{C}| = n_1\boldsymbol{a} + n_2\boldsymbol{b}$, where n_1 and n_2 are integer numbers that are often referred to as chiral indices. Selecting n_1 and n_2 defines the tube radius $r = |\boldsymbol{C}|/2\pi$. For the purpose of illustration, we may select $n_1 = 30$ and $n_2 = 10$, which is equivalent to $r = 6.3$ nm. The corresponding chiral angle $\delta = \cos^{-1}(\boldsymbol{C} \cdot \boldsymbol{a}/|\boldsymbol{C}| \cdot |\boldsymbol{a}|) = 11.8°$.
- Align the unit cell by defining the *x*-axis along the ***a***-direction and letting the plane spanned by ***a*** and ***b*** coincide with the *x*-*z* plane. Subsequently, perform a rotation in this plane to pre-orient ***a*** along the desired direction with a δ angle with the *x*-axis, as we set the ***C*** along the *x*-axis. For our case, the desired direction is along $(x, z) = (r \cdot \sin\alpha_a, -h_a)$, with α_a and h_a given below. Finally, translate the unit cell such that one of the Mg^{2+} ions is centered at (0, 0, 0), and define the set of position vectors for all *L* atoms: $\mathcal{X}^0 = \{\boldsymbol{x}_l | l = 1, \ldots, L\}$.
- For $0° \leq \delta \leq 180°$, the rotational angle or twist between subsequent molecules growing along the ***a*** and ***b*** directions are given by:

$$\alpha_a = \frac{360° \cdot a \cdot \cos\delta}{|C|}, \alpha_b = \frac{360° \cdot b \cdot \cos(\gamma - \delta)}{|C|}$$

and the translational distance or rise for molecules growing along the ***a*** and***b*** directions are given by:

$$h_a = a \cdot \sin\delta, h_b = b \cdot \sin(\gamma - \delta)$$

where the subscript relates to the ***a*** or ***b***direction. Since the signs of these variables depend on the way the tube is built, we will only consider absolute values. For $\delta = 11.8°$, the twists are $\alpha_a = 13.1°$ and $\alpha_b = 3.4°$ and rises are $h_a = 0.30$ nm and $h_b = 0.91$ nm.

Step 2. Tube building through a 2D helix growth. Our chlorosome tube is built starting from the pre-oriented unit cell, by subsequently generating images via translation h and twist rotation α. The matrices used for these transformations are denoted by $T = T^{\boldsymbol{h}}$ and $R = R^{\alpha}$ where $\boldsymbol{h}$ the translation vector and α the rotation angle with respect to the z-axis, respectively. The first molecule in the tube is obtained by translation $T \bullet \boldsymbol{x}$ with $\boldsymbol{h} = (0, -r, 0)$ to all $\boldsymbol{x} \in \mathcal{X}^0$. We denote this set as $\mathcal{X}^1$.

a) Growth along the ***a***-direction: The total number of images generated in this step is n_1. Taking the image $\mathcal{X}^i$ of the previous step, the next image $\mathcal{X}^{i+1}$ is generated by rotation and translation $T \bullet R \bullet \boldsymbol{x}$ for all $\boldsymbol{x} \in \mathcal{X}^i$, with $\alpha = \alpha_a$ and $\boldsymbol{h} = (0, 0, -h_a)$. This constitutes the basic helix along the ***a***-direction on the tube.

b) Growth along the ***b***-direction: Next, this basic helix is copied along the ***b***-direction. Starting from each of the n_1 images $\mathcal{X}^i (i = 1, \ldots, n_1)$ that have been grown along the ***a***-direction, a new image $\mathcal{X}^{i+n_1}$ is generated by rotation and translation, *i.e.*, $T \bullet R \bullet \boldsymbol{x}$, for all $\boldsymbol{x} \in \mathcal{X}^i (i = 1, \ldots, n_1)$, for a fixed angle $\alpha = -\alpha_b$ and vector $\boldsymbol{h} = (0, 0, h_b)$. This process constitutes two helices on the tube. The same procedure is then applied in an iterative fashion to generate new helices by rotation and translation, with $\mathcal{X}^{i+j \cdot n_1}$ being imaged in $\mathcal{X}^{i+(j+1) \cdot n_1}$ for $i = 1, \ldots, n_1$ and $j \in \mathbb{N}$. By construction, $\mathcal{X}^1$ and $\mathcal{X}^{n_1 \cdot n_2}$ relate to positions in neighboring unit cells on the lattice, and the total length of the helical assembly can be tuned by the number of helix copies $N_{\text{duplicates}}$ along the ***b***-direction. Finally, this assembly is truncated at the bottom and top to provide a cylinder of a predefined length.

Molecular dynamics simulations

All MD simulations were conducted with the Gromacs software *in vacuo* (Abraham et al., 2015), with periodic boundary conditions applied along all dimensions. We used the OPLS-AA force field (Kaminski et al., 2001) and we restrained the Mg ion in the macrocycle of each BChl *c* molecule by adding four Mg–N bonds. The Lennard-Jones nonbonded interaction parameters between Mg and O were tuned to maintain an 0.21 nm Mg-O coordination distance (Karki and Roccatano, 2011). Charge parameters were further refined by the RESP method (Cornell et al., 1993), while electrostatic interactions were calculated by a particle-mesh Ewald method (Essmann et al., 1995). We performed NVT simulations, maintaining the temperature by the V-rescale thermostat (Bussi et al., 2007). As mentioned in the body, all tube structures were simulated for 5 ns at 50 K and sequentially another 5 ns at 300 K. Such simulation protocol has been used in our previous chlorosome studies (Li et al., 2018,2019).

Optical spectra calculation

We adopt the Frenkel Exciton Hamiltonian to compute the absorption, linear dichroism (LD) and circular dichroism (CD) spectra of the aggregates (Li et al., 2019; Prokhorenko et al., 2003). Generally, the excited-state properties of an assembly of N molecules are represented by a $N \times N$ (Frenkel) Hamiltonian matrix, with diagonal entries provided by the molecular site energies and off-diagonal entries by the intermolecular electronic coupling strengths. In our approach, we assume that the surroundings of each BChl molecule in the stack are equivalent, and thus we fix the site energy to a common value $\nu = 15390\ cm^{-1}$ that was determined for the Q_y-transition of isolated BChl *c* in methanol (Prokhorenko et al., 2003). In contrast to most treatments, however, we include molecular information in the off-diagonal entries J_{ij} of the matrix that represent the electronic coupling between molecules i and j. In particular, we use the standard point-dipole approximation (PDA) to determine the coupling strength J_{ij} in terms of the spatial separation and relative orientation of (induced) molecular dipoles taken from molecular simulation snapshots. The magnitude of these transition dipole moments is taken to be 5.48 D, as estimated from experimental data (Prokhorenko et al., 2003). The orientation of the these transition dipole moments is taken along the vector connecting two nitrogen atoms (N_I and N_{III}) (Fujita et al., 2012). Calculated stick spectra have been convoluted with normalized Gaussian profiles to mimic the broadening effect that stems from both the static and dynamic disorder present in actual chlorosomes.

Simulation of mechanical properties

In our steered MD simulations, two ends of tubes are loaded with compression along their tube axis. To save computational time, we consider much shorter tubes (20 nm) than the ones used for the determination

of optical spectra. In particular, whereas CD spectra were found length dependent for tubes shorter than 60 nm (Li et al., 2019), the mechanical properties are not expected to vary significantly for the considered deformations. When pulling, molecules in the top 5 nm part of the tube are grouped together as the pull group, whereas molecules in the bottom 5 nm part of the tube are immobilized. A spring with a spring constant of 5000 kJ mol^{-1} nm^{-2} is attached to the center of mass of the pull group and pulled downward along the tube axis at a constant velocity 5 $\times$ 10^{-3}nm ps^{-1} for a total of 1 ns in each system. We carefully analysed results for different pull velocities to select a proper value. The force on the spring F as well as the variation of the distance between the center of the mass of the two groups $\Delta L = |L - L_0|$ (L_0 is the distance for a non-compressed tube at $t = 0$) are recorded. With the slope fitted from the linear part of the F-ΔL curve, *i.e.*, the part that relates to a fully elastic response, the axial modulus Υ can be calculated as: $\Upsilon = \frac{\sigma}{\varepsilon} = \frac{F/A}{\Delta L/L_0} = \frac{F}{\Delta L}(L_0/A)$, with A the area of tube cross section.